ARTICLE

Nanoscale Thermal AFM of Polymers: Transient Heat Flow Effects

Joost Duvigneau, Holger Schönherr,[†,*] and G. Julius Vancso*

MESA[+] Institute for Nanotechnology and Faculty of Science and Technology, Department of Materials Science and Technology of Polymers, University of Twente, P.O. Box 217, 7500 AE Enschede, The Netherlands. [†]Current address: Department of Physical Chemistry I, University of Siegen, Adolf-Reichwein-Str. 2, 57076 Siegen, Germany.

ABSTRACT Thermal transport around the nanoscale contact area between the heated atomic force microscopy (AFM) probe tip and the specimen under investigation is a central issue in scanning thermal microscopy (SThM). Polarized light microscopy and AFM imaging of the temperature-induced crystallization of poly(ethylene terephthalate) (PET) films in the region near the tip were used in this study to unveil the lateral heat transport. The radius of the observed lateral surface isotherm at 133 °C ranged from 2.2 ± 0.5 to 18.7 ± 0.5 μm for tip−polymer interface temperatures between 200 and 300 °C with contact times varying from 20 to 120 s, respectively. In addition, the heat transport into polymer films was assessed by measurements of the thermal expansion of poly(dimethyl siloxane) (PDMS) films with variable thickness on silicon supports. Our data showed that heat transport in the specimen normal (*z*) direction occurred to depths exceeding 1000 μm using representative non-steady-state SThM conditions (*i.e.*, heating from 40 to 180 °C at a rate of 10 °C s^{-1}). On the basis of the experimental results, a 1D steady-state model for heat transport was developed, which shows the temperature profile close to the tip−polymer contact. The model also indicates that ≤1% of the total power generated in the heater area, which is embedded in the cantilever end, is transported into the polymer through the tip−polymer contact interface. Our results complement recent efforts in the evaluation and improvement of existing theoretical models for thermal AFM, as well as advance further developments of SThM for nanoscale thermal materials characterization and/or manipulation *via* scanning thermal lithography (SThL).

KEYWORDS: nanoscale thermal analysis · scanning thermal microscopy · AFM · thermal gradient · heat flow

*Address correspondence to schoenherr@chemie.uni-siegen.de, g.j.vancso@tnw.utwente.nl.

Received for review July 16, 2010 and accepted October 14, 2010.

Published online October 27, 2010. 10.1021/nn101665k

Nanoscale thermal analysis (NanoTA) is an emerging technique in nanotechnology for the determination of surface transition temperatures of materials with high spatial resolution, complementing well-established bulk methods, such as differential scanning calorimetry (DSC), thermomechanical analysis (TMA), and dynamic mechanical analysis (DMA).[1−5] In addition, NanoTA has found applications in tip-based nanofabrication.[6−8]

NanoTA relies on the use of heatable atomic force microscopy (AFM) probes that possess typical tip radii of curvature of 30 nm or less and are equipped with a resistive Joule heater, which is embedded at the cantilever end.[9,10] As an expansion of earlier scanning thermal microscopy, NanoTA promises to yield access to surface transition temperature characteristics of materials at a spatial resolution of 100 nm or better. Originally, these heatable AFM probes were introduced for the development of high density data storage devices.[11−13] These devices, which function *via* nanoscale *thermomechanical* material manipulation, have been very recently expanded to create 2D and even 3D lithographic structures.[14,15] In their recent papers, Knoll and co-workers have reported on the 3D patterning in polymer resist layers using scanning thermal lithography (SThL).[14,15] Their 3D reproduction of a world map in a poly(phthalaldehyde) film also demonstrated the possible high throughput of this patterning technique with ~40 nm resolution or better. In addition to thermomechanical material manipulation, SThL has proven its feasibility in localized *thermochemical* surface functionalization and subsequent derivatization for the development of (bio)sensors.[16−20]

For the accurate and precise thermal characterization and manipulation of materials on the nanoscale, the long- and short-range temperature gradients that arise from the heated cantilever and extend into its surrounding must be understood. To date, most work that addressed these thermal gradients relied on the use of (over)simplified theoretical models and simulations *without* complementing direct experimental support. Due to the overall complex geometry of the cantilever heat source, which is positioned relatively far away from the surface, the resulting thermal transport covers different regimes.[21,22]

Figure 1 shows a front view of the cantilever end of a heated thermal probe in con-

tact with a polymer film on a solid substrate. The integrated heater area is maintained at a preset temperature of T_H, set by applying a voltage over the cantilever legs. According to calculations of King and coworkers,[1] approximately 20% of the total power generated at the heater area (on the order of a few milliwatts) is lost to the surrounding atmosphere above the cantilever ($q_{ambient}$). A large fraction of the generated power is dissipated *via* the air gap ($d_{gap} \sim 4$ μm) between cantilever legs and polymer film (q_{gap}). The calculations show that only about 0.1% of the generated power is conducted through the probe−polymer contact (q_i). Radiative heat transport was concluded to be insignificant.[23,24] These different pathways of heat conduction contribute to a different extent and at different length scales to the heating of the substrate. Calculations by Hoerber and coworkers[25] showed, for example, that substrates with good heat conductivity are substantially less heated as compared to poor thermal conductors when they are brought into contact with the heated probe. The surface temperature increase for glass ($\lambda \sim 1$ W m^{-1} K^{-1}) and silicon ($\lambda \sim 350$ W m^{-1} K^{-1}) substrates below a cantilever heated to 440 °C ($d_{gap} = 0.5$ μm) was calculated to be 100 and 20 °C, respectively.

Furthermore, Hoerber *et al.* showed that the temperature at the probe−substrate interface (T_i) strongly depends on the thermal conductivity of the surface under investigation. For a tip radius of 10 nm and the cantilever heated to 440 °C, their model predicted a tip interface temperature of ~320 °C for glass and ~100 °C for silicon surfaces. Nelson and King confirmed these trends in calculations that show a correlation of T_i with the ratio of substrate to tip thermal conductivity.[21] In agreement with the results by Hoerber *et al.*, these results revealed that a significantly shallower thermal gradient exists within the tip for low conductivity materials compared to high conductivity materials. King and coworkers performed another interesting finite element simulation of a cantilever positioned in air.[26] During heating with a power of 8 mW for 100 μs, the temperature gradient in the direction of the principal axis of the cantilever covered >120 μm. The air close to the heater area reached temperatures >400 °C.[26] In addition, these simulations convincingly illustrated the anticipated cantilever shape effect on the heat diffusion from the cantilever to its surrounding.

While abundant simulation data can be found in the literature, experimental confirmation remains scarce. King and co-workers[27] estimated that about 75% of the power generated in the probe reaches the substrate directly below the heated cantilever using a ~140 nm wide platinum resistance thermometer fabricated on a SiO_2 surface. These data are very close to the simulation results mentioned above. These measurements, however, did not provide insights in the lateral evolution of thermal transport, most likely due to the strong dependency of the nanothermometer response as a function of the cantilever orientation with respect to the thermometer position.[27] In addition, the experimental results are limited to a relatively good thermal conductor (SiO_2), whereas in many applications, polymers (which are poor thermal conductors) and especially polymer thin films are applied. For this important class of materials, a substantial increase in surface temperature below the heated cantilevers is expected. Hence this problem was studied in detail in this article.

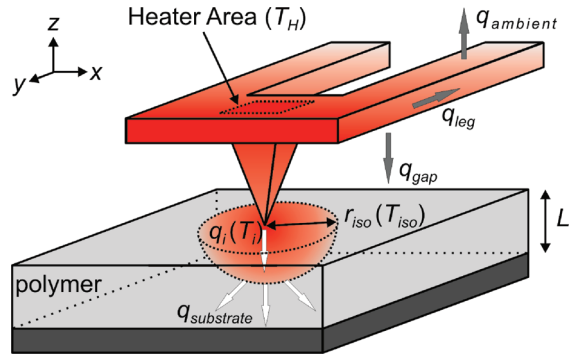

Figure 1. Schematic front view of a batch fabricated heatable AFM probe in contact with a polymer film on a solid substrate. The integrated heater area, positioned above the tip, is brought to a preset temperature T_H, which is controlled by applying a voltage over the cantilever legs. The resulting heat fluxes (q) are represented by the white and gray arrows, indicating the different pathways of heat loss from the heater area.

As shown, we measured the range of the temperature gradient in SThM (*i*) in the lateral direction close to the tip−sample contact (<10 μm) and (*ii*) in the vertical direction far away from the tip−sample contact into polymer films ($z \gg 100$ μm) during *non-steady-state* heating conditions. The results obtained are of interest for the evaluation and improvement of existing theoretical models for SThM, as well as for further developments of SThM-based approaches aiming at high-resolution thermal material characterization and/or manipulation.

RESULTS AND DISCUSSION

We assessed the temperature gradients in scanning thermal microscopy using two polymer systems (*i.e.*, amorphous PET films and cross-linked PDMS elastomer films with varying thickness values). PET quenched from the melt to an amorphous state was chosen as crystallization will proceed radially upon heating with a thermal AFM probe to temperatures >133 °C. Cross-linked PDMS elastomer was chosen as it exhibits a high thermal expansion coefficient ($\alpha \sim 200 \times 10^{-6}$ °C^{-1})[28] and good thermal stability.

The corresponding thermal gradients were estimated from an analysis of the lateral dimensions of crystallites obtained in the heat-induced crystallization of PET (Figure 2) and the variation in the thermal expansion of PDMS films as a function of film thicknesses on silicon (Figure 3).

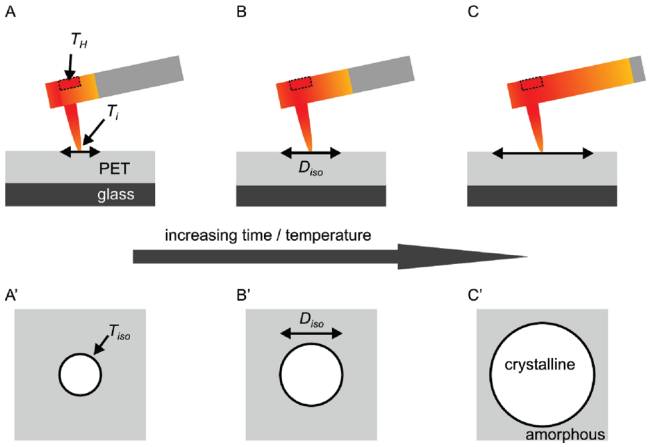

Figure 2. Schematic cross-sectional side view of a heated AFM probe in contact with an amorphous PET film prepared by rapid cooling PET from the melt to room temperature (the cantilever is mounted at an inclination angle of ~12°). The thermal gradient, marked by the double-headed arrows on the PET surface, underneath the heated AFM probe induces localized crystallization as long as the temperature remains above the threshold temperature for crystallization of PET (~133 °C). The resulting size of the semicrystalline domains ($D_{iso} = 2r_{iso}$) depends on the holding time and the probe temperature (T_i) (A–C). Bottom: schematic top view images of the corresponding semicrystalline domains (A′–C′). The outer semicrystalline domain boundary can be considered as an isotherm of temperature T_{iso} (~133 °C).

Heat-Induced Localized PET Crystallization. To analyze the lateral heat transport, heated AFM probes were brought into contact with an amorphous PET film. Here they induce the formation of spherulite-like crystallites (Figure 4) when the substrate temperature reaches temperatures above the threshold temperature for crystallization (T_c). The evaluation of the size of the semicrystalline domains formed (diameter $D_{iso} = 2r_{iso}$) as a function of T_i and heating time provides insight in the lateral evolution of T_c in the form of an isotherm (T_{iso}) (Figure 5; compare also Figure 1).

For a comparison, T_{iso} was determined as 133 °C from the onset of crystallization of amorphous PET samples observed in DSC heating traces (Supporting Information). Figure 5 shows AFM contact mode deflection images acquired after heated AFM probe induced growth of semicrystalline PET domains at $T_i = 250$ °C for different holding times. The semicrystalline nature of the domains was confirmed with polarized light microscopy (see Figure 4) and local NanoTA melting point measurements. The observed birefringence in polarized light microscopy revealed the nucleation and growth of many small crystallites that possess negative birefringence and resemble in some areas crude spherulites. From the NanoTA experiments, a typical melting transition of 188 ± 3 °C was determined, independent of the radial position within the semicrystalline domain. This marked deviation from the bulk melting point (T_m(DSC) = 235 ± 5 °C) is attributed to (*i*) the short crystallization times in a non-uniform temperature field, which results in the formation of imperfect semicrystalline domains, as well as to (*ii*) the known complex melting behavior of PET.[29,30]

For the determination of D_{iso}, the semicrystalline domains were assumed to be circular in shape. Most of the deviations from the assumed circularity were observed at that side of the semicrystalline domains (see Figure 5) that was closest to the cantilever base for practically the entire range of holding times and tip temperatures used. This deviation is attributed to the fact that the cantilever is mounted at an inclination angle of 12° with respect to the cantilever holder plane. Since about 75% of the heat generated in the cantilever legs reaches into the underlying polymer film according to simulations by King and co-workers,[27] the increased separation distance at a few micrometers distance away from the tip–polymer contact point is sufficient to cause a substantial decrease in surface temperature. In addition, the tip–polymer contact point was typically not in the center of the domains formed but was closer to the cantilever end. The noncircular shapes of the domains are therefore in agreement with the notion that

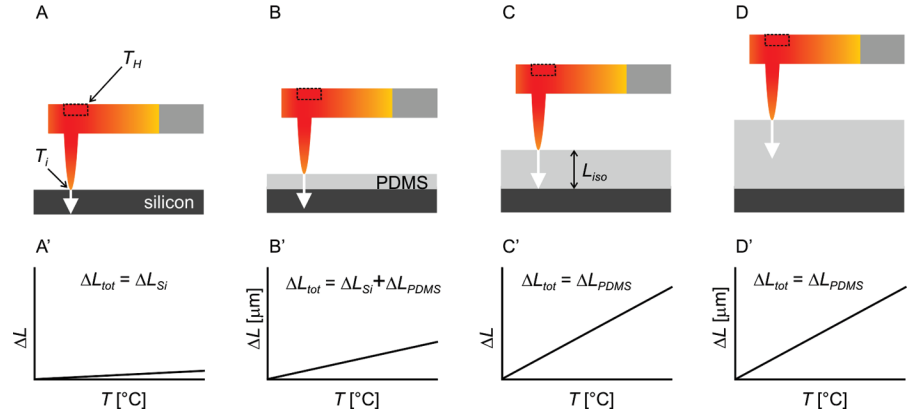

Figure 3. Schematic cross-sectional side view of a heated AFM probe in contact with a silicon substrate (A) or PDMS films with increasing thicknesses on silicon substrates (B–D) (the cantilever is mounted at an inclination angle of ~0°). The non-steady-state heat penetration depth directly below the tip–sample contact at time *t* and temperature *T*(*t*) during temperature scans is indicated by the white arrow (*z* direction). Graphs A′ to D′ show the respective schematic thermal expansion (Δ*L*) *vs* temperature plots. Under conditions shown in C, the heat flux is not sufficient to raise the temperature at the silicon PDMS interface, and as a consequence, the thermal expansion for even thicker films as a function of temperature becomes independent of the PDMS film thickness (*D*).

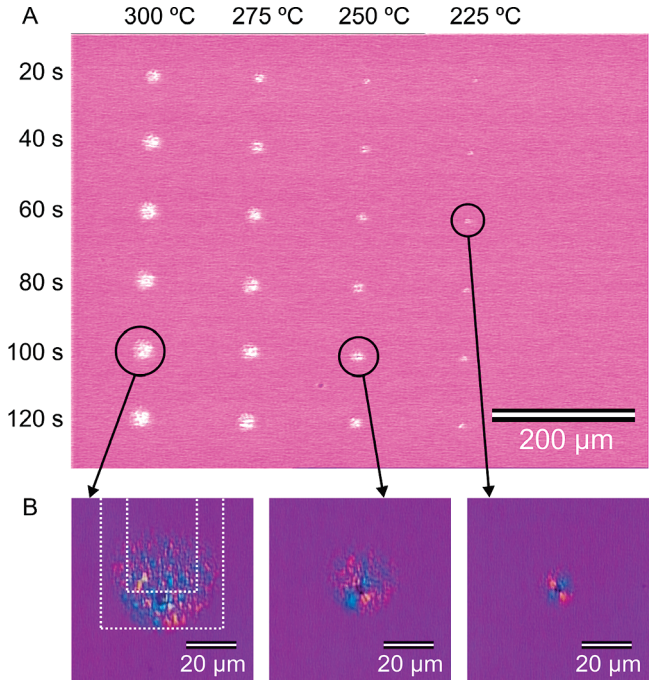

Figure 4. Polarized light microscopy images (using crossed polars and a lambda) of semicrystalline PET domains formed in the surface region near the heated AFM probe tip. (A) Low-magnification overview image of part of the formed domains. The tip temperatures and heating times are denoted at the top and left side of the image, respectively. Note: In A, the color balance was adjusted to enhance the contrast between the amorphous PET and semicrystalline PET domains. (B) Higher magnification images of the corresponding crystals within the black circles in A (turned 90° clockwise with respect to A). The observed birefringence is a result of the semicrystalline morphology within these domains. The cantilever orientation is schematically shown in B (left image, dotted lines, not to scale). Note: Localized crystallization was also observed in experiments in which the heated cantilever was positioned 1 μm above the PET film.

most of the heat is conducted into the cantilever legs from where it is dissipated over the air gap between the cantilever and polymer film.

Figure 6A shows a plot of D_{iso} as a function of time for preset temperatures between 200 and 300 °C. The observed values of D_{iso} range from ~2.4 ± 1.0 to ~37.4 ± 1.0 μm for 20 s at 200 °C and 120 s at 300 °C, respectively. Following the initial increase in rate of propagation of the lateral isothermal boundary, the observed rate reaches a plateau value (D_{max}). The obtained values of D_{max} are plotted *versus* probe temperature in Figure 6B.

PDMS Film Thickness Dependent Thermal Expansion. To analyze the heat transport into polymer films in the *z* direction under a heated NanoTA probe, the film thickness dependent thermal expansion of PDMS films on silicon substrates was investigated (Figure 3). During conventional NanoTA measurements, the deflection signal is monitored as a function of temperature after bringing the probe into contact with the polymer film. The force feedback is switched off during such an experiment. When the temperature is ramped up, the polymer film thermally expands. This results in an increase of the deflection signal (*i.e.*, the cantilever bends up). Once a transition temperature (*e.g.*, T_g or T_m) is reached, a pronounced drop in the deflection signal is observed. The onset of the transition is assigned to the temperature at which the slope of the deflection *versus* temperature plot becomes zero. The upward bending of the cantilever significantly increases the load (normal force) applied by the cantilever on the film before the transition temperature is reached. The increase, which may amount to several 100 nN (a factor of 30), in-

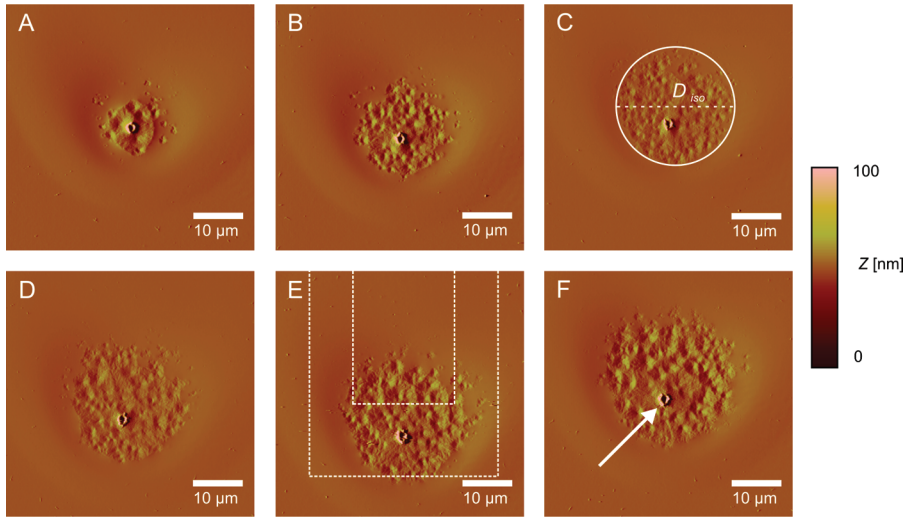

Figure 5. AFM contact mode deflection images of semicrystalline domains of PET grown by localized crystallization induced by the heated probe tip. A nominal tip temperature of 250 °C was kept constant for 20 s (A), 40 s (B), 60 s (C), 80 s (D), 100 s (E), and 120 s (F). D_{iso} was measured as the diameter of a circle fitted to the contour of the semicrystalline domain as depicted in C. The cantilever orientation is schematically shown in E (dotted lines, not to scale). The white arrow in F points to the residual indent at the tip−PET contact point.

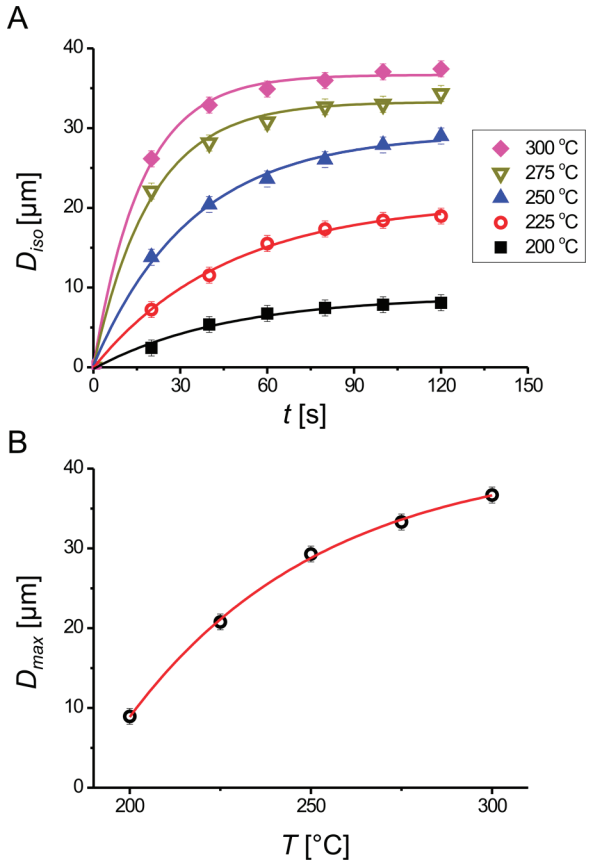

Figure 6. (A) D_{iso} as a function of time for heated AFM probe tip induced growth of semicrystalline PET domains with preset probe temperatures (T_i) in the range of 200 to 300 °C. (B) Maximum PET domain size (D_{max}) as a function of the probe temperature. The solid lines are exponential fits to the data and serve as a guide for the eye.

creases the tip−polymer contact area and hence affects the thermal transport through the probe. To avoid this increase in forces, the AFM was operated in a force feedback mode in our experiments, maintaining a constant force of 10 nN. To detect the thermal expansion of the polymer film, the Z-sensor position of the closed loop feedback system was monitored, which provides a direct measure of the thermal expansion (ΔL) of the film (Figure 3A′−D′).

It is well-known that the linear thermal expansion (ΔL) of material A (*e.g.*, PDMS) with thickness L_A on top of material B (*e.g.*, silicon) with thickness L_B with a total thickness of L in a uniform temperature field (ΔT) can be expressed as the combined thermal expansion of both materials.[31−33] Despite the fact that the temperature field in its surrounding is *non-uniform* and as such becomes a function of time (t) and position (z), the observed thermal expansion at time t_1 is the combined thermal expansion of both the material under investigation and the underlying material. This scenario only holds if the heat transport is sufficient to induce an increase in temperature in material B. When this requirement is no longer met, only material A contributes to the observed thermal expansion and hence ΔL becomes independent of L_A (compare Figure 3).

Thus, by measuring the film thickness dependence of the thermal expansion of elastomeric PDMS films ($\alpha \sim 200 \times 10^{-6}$ °C^{-1})[28] on silicon substrates ($\alpha \sim 3 \times 10^{-6}$ °C^{-1})[34] by NanoTA measurements, insight in the length scale of heat transport in the z direction is obtained during non-steady-state conditions typically used in NanoTA. The over 60-fold higher thermal expansion coefficient of PDMS compared to silicon provides a good resolution for determining T_{iso}.

Figure 7A shows the measured thermal expansion as a function of temperature for temperature ramps between 40 and 180 °C at 10 °C s^{-1} on PDMS films on silicon with film thicknesses ranging from 0 to 5×10^{-3} m. The temperature range and ramp rate are representative for typical NanoTA measurements.

It can be seen in Figure 7A that the measured thermal expansion is very small for a bare silicon surface, whereas it increases significantly when PDMS films are locally heated. Finally, for the thicker films, the thermal expansion becomes independent of the film thickness. The PDMS film thickness at which this occurs was calculated from a plot of the observed thermal expansion as a function of the PDMS film thickness (Figure 7B). The thermal expansion data were plotted for temperature increments of 10 °C. L_{iso} was determined for each corresponding temperature from the exponential fits of the experimental data. Figure 8 shows L_{iso} for the respective temperatures with an interval of 10 °C. During the applied non-steady-state localized surface heating, the length scale of non-steady-state thermal conduction in the PDMS films directly below the heated cantilever ranges from ~465 to ~1350 μm. The fit to the data suggests that L_{iso} is proportional to $T^{0.33}$ within the temperature range investigated.

The exact temperature profile at these length scales is unknown; however, a steep thermal gradient close to the probe−sample contact point can be expected.[3,35] Despite the unknown exact thermal gradient, the averaged temperature increase is expected to be on the order of approximately 10 °C, based on the measured thermal expansion of the thicker PDMS samples heated to 180 °C (see Supporting Information). The length scale of heat transport was verified in measurements with 100 μm diameter thermocouples embedded in PDMS samples at 0, 500, and 1150 μm depth. Upon increasing the probe temperature (T_i) from 40 to 180 °C at a heating rate 10 °C s^{-1}, the embedded thermocouple detected a measurable increase in temperature (see Supporting Information). Subsequent heating and cooling cycles did not show any hysteresis. Despite the semiquantitative nature of the data acquired, the observed thermocouple response at depths over 1000 μm confirms the observed length scale of heat transport for the measured L_{iso} calculated from the thermal expansion data on PDMS. The normalized tem-

perature response for the depths investigated revealed a sharp drop in temperature close to the tip−sample contact, which is in agreement with our expectations. Interestingly, the thermocouples also showed an increase in temperature when they were embedded at a depth of 500 μm, while the heated cantilever was positioned 100 μm above the PDMS film (*i.e.*, not in physical contact with the PDMS surface). No change in temperature was detected when the heated cantilever was positioned 1000 μm above the PDMS surface. Furthermore, an increased temperature was observed when the heated cantilever was in contact with the PDMS film and positioned 500 μm away in the lateral (*x*) direction from the initial contact point straight above the embedded thermocouple. These results once more confirm that for typical conditions used in NanoTA measurements heat transport in *z* direction extends over distances >1000 μm for polymers.

Simplified Steady-State 1D Model. The observation of the 133 °C isotherm at micrometer length scales from the tip−probe contact points for T_i between 200 and 300 °C suggests that there is a very steep thermal gradient close to the tip, when it is in contact with the polymer film. This is confirmed by the calculated average temperature increase of ~10 °C for the PDMS film, which extends over 1000 μm in the *z* direction for a probe temperature of 180 °C. On the other hand, as discussed above, PDMS, as well as PET experiments revealed that surface heating with the cantilever positioned slightly above the polymer films induces an increase in surface and subsurface temperature. Therefore, substantial surface heating at these distances must be taken into account. The existence of a plateau value in Figure 6A suggests that after 100 s a quasi-steady-state is reached for the preset probe temperatures used. These isothermal points at known distances from the tip−sample contact point were taken into account in a simplified 1D model for *steady-state* spherical heat conduction (Figure 9). The model is based on the following assumptions:

- The system is in the steady state.
- The tip−PET interface is a hemisphere with preset temperature (T_i).
- Phase changes can be neglected.
- Convective surface cooling can be neglected.

The steady-state heat rate *q* conducted through the PET hemisphere can be described as follows:[36]

where r_1 and r_2 denote the radii at steady surface

$$q = \frac{2\pi k r_1 r_2}{r_1 - r_2}(T_1 - T_2) \qquad (1)$$

temperatures of T_1 and T_2, respectively, with $T_1 > T_2$ and *k* is the thermal conductivity of PET (0.24 W m^{-1} K^{-1}).[37] The temperature gradient in the hemisphere can be calculated as

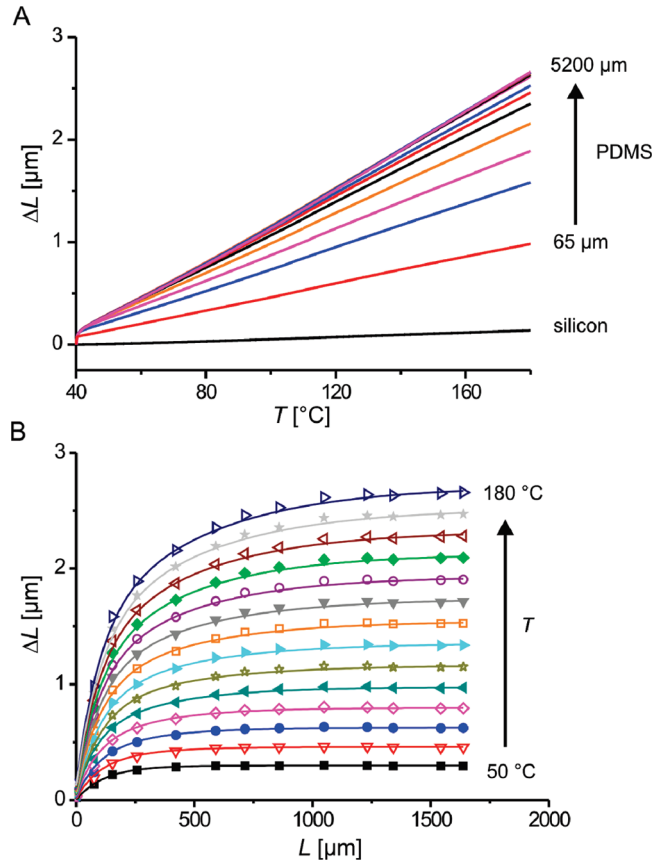

Figure 7. (A) Thermal expansion *vs* temperature plots obtained with heated AFM probe temperature scans from 40 to 180 °C with a temperature ramp of 10 °C s^{-1} on PDMS films with different thicknesses. (B) Thermal expansion *vs* PDMS film thickness for temperatures ranging from 50 to 180 °C measured during the temperature ramps presented in A. The solid lines in B are exponential fits to the data and serve as a guide for the eye.

$$\frac{T - T_2}{T_1 - T_2} = \frac{1 - r_2/r}{1 - r_2/r_1} \qquad (2)$$

where *r* is the radius at temperature *T* with $T_1 > T > T_2$ and $r_1 < r < r_2$.

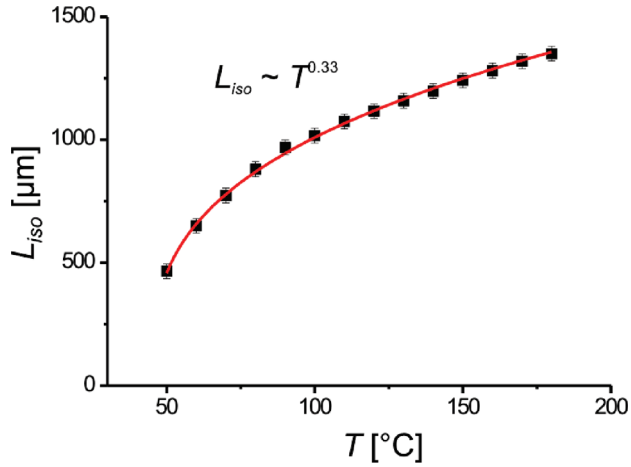

Figure 8. L_{iso} as a function of temperature during NanoTA temperature ramps on PDMS films from 40 to 180 °C at a heating rate of 10 °C s^{-1}.

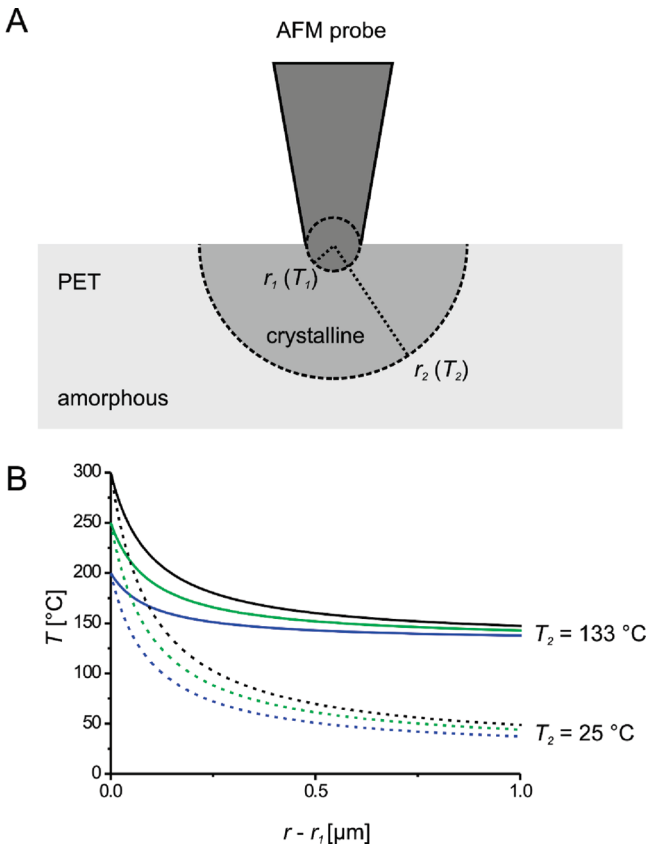

Figure 9. (A) Simplified schematic of a heated AFM probe in contact with an amorphous PET film (the tip size and the radii r_1 and r_2 are not drawn to scale). (B) Calculated steady-state temperature profiles around a heated AFM tip with preset temperatures ($T_1 = T_i$) of 200, 250, and 300 °C. The radial distance away from the probe−polymer interface is represented by $r - r_1$. The solid lines represent the calculated temperature profiles when surface heating ($T_2 = 133$ °C) in the vicinity of the tip is taken into account, whereas the dotted lines assume no significant surface heating in the proximity of the tip ($T_2 = 25$ °C).

In this model, r_1 represents the tip−PET interface contact point assuming a spherical contact area. The contact radius r_1 was estimated from cross-sectional analysis of the probe−polymer contact point observed in the AFM height images by fitting a spherical tip shape in the residual indent (see for example Figure 5F). AFM height images for heating times of 100 and 120 s for all preset temperatures were taken into account. For r_1, a value of 220 ± 40 nm was calculated. This value of r_1 is large compared to the typical tip radius stated by the manufacturer for these heatable AFM probes (<30 nm). The discrepancy is explained by the fact that while growing the semicrystalline domains the temperature is well above the T_g of PET (T_g ~73 °C). Hence the probe penetrates the polymer film substantially, resulting in an increased contact area. Analyzing AFM height images obtained by scanning an array of sharp tips[38] with a new and an extensively used heatable AFM probe provided tip radii on the order of 30 and 100 nm. On the basis of these numbers, a value of 100 nm will be used for the following calculations. It is assumed that for most applications with these heatable AFM probes this number leads to an overestimate for the tip−sample contact area. The value of r_2 was calculated as 0.5 × D_{max}. Figure 9B shows the temperature distribution calculated from eq 2 for preset probe temperatures of 200, 250, and 300 °C with and without taking substantial surface heating into account. The use of the isothermal boundary at 0.5 × D_{max} to calculate the thermal gradient from the tip−sample interface is justified based on the observed micrometer range crystallization of PET when there was no contact between the heated cantilever and PET. Furthermore, for an increased r_2 up to 1000 μm, no significant change in the thermal gradient close to the tip−PET contact point was observed, which once more justifies its use as a boundary condition in our calculations.

In Figure 9, a very sharp decrease in temperature is observed close to the tip−polymer contact point regardless whether substrate heating is taken into account or not. Approximately 90% of the temperature drop occurs within 1 μm from the tip−polymer contact point. Less steep thermal gradients are observed when substantial surface heating is taken into account. This will adversely influence the resolution of thermal scanning probe-based material characterization or manipulation. The heat flux from the heated probe through the tip−polymer interface (q_i, Figure 1) was calculated to be ~1.4, ~1.1, and ~0.8% of the power generated in the heater area in the cantilever end at a tip temperature of 300, 250, and 200 °C, respectively. These numbers are in reasonable agreement with calculations from King and co-workers in which 0.1% of the power generated was found to travel through the probe−material interface.[1] Lowering of the large contact radius (r_1) to 30 nm will substantially lower the calculated heat flux through the tip−polymer interface to approximately 0.3% of the total power generated at the cantilever heater area (T_i = 250 °C).

This simplified model does not allow one to model the thermal transport completely or to predict accurate thermal gradients. However, the experimental results presented above revealed long-range heat transport over more than 1000 μm within polymeric materials under typical NanoTA conditions. Short contact times at relatively low temperatures already revealed thermal transport over several hundreds of micrometers and the existence of a very sharp temperature gradient close to the tip.

Several examples are known in literature on how to avoid substantial surface heating in different research areas where heatable AFM cantilevers are used. First we would like to mention the somewhat trivial solution for thermal scanning probe lithography, which is fast scanning while reducing the contact area of the tip with the polymer material.[39] Second, in applications such as nanoDSC, the application of an AC current instead of a DC current to the cantilever induces an oscillating temperature that significantly reduces the thermal transport in the surface below the heated cantilever.[40]

The experimental results presented here could be used in future research to further improve (existing) models for thermal transport from heated AFM cantilevers in contact with polymer surfaces, as well as in optimizing the experimental conditions for heated cantilever-based AFM approaches.

CONCLUSIONS

The length scale of thermal transport in both lateral and vertical directions arising from heated AFM cantilevers in contact with polymer films was experimentally investigated. Heated probe induced crystallization of amorphous PET resulted in the formation of near-circular semicrystalline domains in the tip-near region. The periphery of the domain boundaries was considered as a surface isotherm at 133 °C. The radii of the observed lateral surface isotherms ranged from 2.2 ± 0.5 to 18.7 ± 0.5 μm as was revealed with AFM and polarized light microscopy for heated AFM probe tip temperatures between 200 and 300 °C and contact times varying from 20 to 120 s. The heat transport into polymer films was estimated from thermal expansion measurements of silicon-supported PDMS films with variable thickness. Our data showed that heat transport in the *z* direction occurred to depths over 1000 μm using representative non-steady-state SThM conditions (*i.e.*, heating from 40 to 180 °C at 10 °C s^{-1}). This was semiquantitatively confirmed by temperature measurements with thermocouples embedded in PDMS films at depths comparable to the observed length scale of thermal transport. A simplified model for 1D steady-state spherical heat transport showed a steep temperature gradient close to the tip contact point. The temperature gradient was less steep when surface heating was taken into account. The experimental evaluation of thermal transport from heated AFM cantilevers in contact with polymer films will be of use for the further development of heated cantilever-based AFM approaches as well as for the validation of theoretical models.

MATERIALS AND METHODS

PDMS Films. The films were prepared from Sylgard-184 (Dow Corning, Midland, MI). Typically 5:1 (w/w) elastomer to curing agent mixtures were degassed by applying a vacuum for 20 min in two subsequent pumping cycles before pouring them carefully over a silicon wafer (10 cm diameter, tilted at ~12°, or on horizontally leveled 1 cm × 1 cm silicon pieces). Following two more degassing cycles, the PDMS was cured at 60 °C for 12 h. After cooling to room temperature, the wafer was broken in the middle and marks were made with a scalpel at regular distances for positioning purposes. Copper-constantan thermocouples (5TC-TT-T-36-72, Omega Engineering Inc. Stamford, CT) were embedded in PDMS films at well-defined positions by placing them in the prepolymer solution prior to curing to enhance the thermal contact. The exact depth of the thermocouple with respect to PDMS surface was determined by cross-sectional light microscopy following the NanoTA measurements.

PET Samples. PET granulate (Goodfellow, Huntingdon, UK), deposited between two precleaned microscope glass slides, was molten at 290 °C in a temperature-controlled hydraulic press (Specac, London, UK), while applying a load of ~0.1 ton. After cooling the sample, the top microscopy slide was removed and the remaining PET film was heated again to 290 °C for 5 min to erase the thermal history, before it was quenched to room temperature by quickly removing the film from the hot press and placing it in Milli-Q water (Millipore Synergy system, Billereca, MA). The amorphous PET film was blown dry with a nitrogen stream. The thickness of the resulting PET film was over 1 mm.

Atomic Force Microscopy. AFM measurements were done with a Dimension D3100 AFM operated with a Nanoscope IVa controller (Digital Instruments/Veeco, Santa Barbara, CA) equipped with heatable silicon AFM probes (type AN-2, Anasys Instruments, Santa Barbara, CA). The probe temperature was controlled with a NanoTA2 controlled (Anasys Instruments). Prior to the experiments, the probe temperature was calibrated using polymer melting point standards[41] (polycaprolactone, polyethylene, and poly(ethylene terephthalate) with melting points of 55, 116, and 235 °C, respectively). Tip apexes were characterized using a silicon calibration grating with ultrasharp tips (nominal radius 10 nm, TGT1, NT-MDT, Moscow, Russia).[38]

Thermal Expansion Measurements. The thermal expansion of the PDMS film was measured by recording the Z-sensor position as a function of temperature, while T_i was ramped from 50 to 180 °C with a rate of 10 °C s^{-1} at preselected positions of the sample. During the measurements, a contact load of ~10 nN was applied.

Heat-Induced Crystallization. The local crystallization of PET films was carried out by positioning the heated AFM probe (with T_i ranging from 200 to 300 °C) in contact with the PET film with an initial contact force of ~10 nN for a specified holding time (ranging from 0 to 120 s). Afterward, the probe was withdrawn from the sample and subsequently cooled to room temperature. Contact mode AFM images of the formed semicrystalline domains were captured with the same probe as used in the heating experiments. Tapping mode images of the semicrystalline domains were recorded with PointProbe Plus silicon probes (PPP-NCH, Nanosensors, Neuchatel, Switzerland).

Differential Scanning Calorimetry. DSC measurements on PET bulk samples were carried out with a Perkin-Elmer DSC-7 (Waltham, MA). Heating and cooling traces, between 30 and 300 °C, of amorphous PET samples were recorded at 10 °C min^{-1}.

Polarizing Optical Microscopy. Images of the PDMS films (cross sectional) and PET semicrystalline domains were recorded with an Olympus BX60 microscope. The PET semicrystalline domains were examined between crossed polars with a lambda plate (γ 530 nm, U-TP 530, Olympus, Zoeterwoude, The Netherlands) inserted between the specimen and analyzer.

Acknowledgment. The authors are grateful to Goodfellow (Huntingdon, UK) for donating the PET sample. This work was supported by NanoImpuls/NanoNed, the nanotechnology program of the Dutch Ministry of Economic Affairs (Grant TPC.6940) and by the NWO Middelgroot Grant 700.54.102.

Supporting Information Available: Differential scanning calorimetry heating and cooling traces of PET used for the determination of T_{iso}, as well as representative NanoTA data of the formed semicrystalline domains are shown. In addition, the calculation of the average temperature increase within the PDMS film (*z*) is shown. Furthermore, a light microscopy image of a thermocouple embedded in a PDMS film is presented together with a table presenting the measured changes in temperature for the different experimental probe−thermocouple alignments. This material is available free of charge *via* the Internet at http://pubs.acs.org.

REFERENCES AND NOTES

1. King, W. P.; Saxena, S.; Nelson, B. A.; Weeks, B. L.; Pitchimani, R. Nanoscale Thermal Analysis of an Energetic Material. *Nano Lett.* **2006**, *6*, 2145–2149.
2. Nelson, B. A.; King, W. P. Measuring Material Softening with Nanoscale Spatial Resolution Using Heated Silicon Probes. *Rev. Sci. Instrum.* **2007**, *78*, 023702.
3. Zhou, J.; Berry, B.; Douglas, J. F.; Karim, A.; Snyder, C. R.; Soles, C. Nanoscale Thermal-Mechanical Probe Determination of 'Softening Transitions' in Thin Polymer Films. *Nanotechnology* **2008**, *19*, 495703.
4. Gotzen, N. A.; Van Assche, G.; Ghanem, A.; Van Ingelgem, Y.; Hubin, A.; Van Mele, B. Micro- and Nano-thermal Analysis Applied to Multi-layered Biaxially-Oriented Polypropylene Films. *J. Therm. Anal. Calorim.* **2009**, *95*, 207–213.
5. Mueller, T. Quantitative Nanoscale Characterization. *Mater. Today* **2009**, *12*, 40–43.
6. Basu, A. S.; McNamara, S.; Gianchandani, Y. B. Scanning Thermal Lithography: Maskless, Submicron Thermochemical Patterning of Photoresist by Ultracompliant Probes. *J. Vac. Sci. Technol., B* **2004**, *22*, 3217–3220.
7. Hua, Y. M.; Saxena, S.; Clifford, H.; King, W. P. Nanoscale Thermal Lithography by Local Polymer Decomposition Using a Heated Atomic Force Microscope Cantilever Tip. *J. Micro/Nanolithogr. MEMS* **2007**, *6*, 023012.
8. Hua, Y. M.; King, W. P.; Henderson, C. L. Nanopatterning Materials Using Area Selective Atomic Layer Deposition in Conjunction with Thermochemical Surface Modification *via* Heated AFM Cantilever Probe Lithography. *Microelectron. Eng.* **2008**, *85*, 934–936.
9. Chui, B. W.; Stowe, T. D.; Ju, Y. S.; Goodson, K. E.; Kenny, T. W.; Mamin, H. J.; Terris, B. D.; Ried, R. P.; Rugar, D. Low-Stiffness Silicon Cantilevers with Integrated Heaters and Piezoresistive Sensors for High-Density AFM Thermomechanical Data Storage. *J. Microelectromech. S* **1998**, *7*, 69–78.
10. King, W. P. Design Analysis of Heated Atomic Force Microscope Cantilevers for Nanotopography Measurements. *J. Micromech. Microeng.* **2005**, *15*, 2441–2448.
11. Mamin, H. J. Thermal Writing Using a Heated Atomic Force Microscope Tip. *Appl. Phys. Lett.* **1996**, *69*, 433–435.
12. Vettiger, P.; Cross, G.; Despont, M.; Drechsler, U.; Dürig, U.; Gotsmann, B.; Häberle, W.; Lantz, M. A.; Rothuizen, H. E.; Stutz, R.; *et al.* The "Millipede"—Nanotechnology Entering Data Storage. *IEEE Trans. Nanotechnol.* **2002**, *1*, 39–55.
13. Vettiger, P.; Despont, M.; Drechsler, U.; Dürig, U.; Häberle, W.; Lutwyche, M. I.; Rothuizen, H. E.; Stutz, R.; Widmer, R.; Binnig, G. K. The "Millipede"—More Than One Thousand Tips for Future AFM Data Storage. *IBM J. Res. Dev.* **2000**, *44*, 323–340.
14. Gotsmann, B.; Knoll, A. W.; Pratt, R.; Frommer, J.; Hedrick, J. L.; Düerig, U. Designing Polymers To Enable Nanoscale Thermomechanical Data Storage. *Adv. Funct. Mater.* **2010**, *20*, 1276–1284.
15. Pires, D.; Hedrick, J. L.; De Silva, A.; Frommer, J.; Gotsmann, B.; Wolf, H.; Despont, M.; Düerig, U.; Knoll, A. W. Nanoscale Three-Dimensional Patterning of Molecular Resists by Scanning Probes. *Science* **2010**, *328*, 732–735.
16. Szoszkiewicz, R.; Okada, T.; Jones, S. C.; Li, T. D.; King, W. P.; Marder, S. R.; Riedo, E. High-Speed, Sub-15 nm Feature Size Thermochemical Nanolithography. *Nano Lett.* **2007**, *7*, 1064–1069.
17. Wang, D. B.; Kodali, V. K.; Underwood, W. D.; Jarvholm, J. E.; Okada, T.; Jones, S. C.; Rumi, M.; Dai, Z. T.; King, W. P.; Marder, S. R.; *et al.* Thermochemical Nanolithography of Multifunctional Nanotemplates for Assembling Nano-objects. *Adv. Funct. Mater.* **2009**, *19*, 3696–3702.
18. Lee, W. K.; Whitman, L. J.; Lee, J.; King, W. P.; Sheehan, P. E. The Nanopatterning of a Stimulus-Responsive Polymer by Thermal Dip-Pen Nanolithography. *Soft Matter* **2008**, *4*, 1844–1847.
19. Duvigneau, J.; Schönherr, H.; Vancso, G. J. Atomic Force Microscopy Based Thermal Lithography of Poly(*tert*-butyl acrylate) Block Copolymer Films for Bioconjugation. *Langmuir* **2008**, *24*, 10825–10832.
20. Vancso, G. J.; Schön, P.; Duvigneau, J. What's New in Atomic Force Microscopy of Polymers? An Update. *Microsc. Anal.* **2009**, *23*, 5–11.
21. Nelson, B. A.; King, W. P. Modeling and Simulation of the Interface Temperature between a Heated Silicon Tip and a Substrate. *Nanosci. Microsc. Therm.* **2008**, *12*, 98–115.
22. Masters, N. D.; Ye, W. J.; King, W. P. The Impact of Subcontinuum Gas Conduction on Topography Measurement Sensitivity Using Heated Atomic Force Microscope Cantilevers. *Phys. Fluids* **2005**, *17*, 100615.
23. Lee, J.; Wright, T. L.; Abel, M. R.; Sunden, E. O.; Marchenkov, A.; Graham, S.; King, W. P. Thermal Conduction from Microcantilever Heaters in Partial Vacuum. *J. Appl. Phys.* **2007**, *101*, 014906.
24. Kim, K. J.; Park, K.; Lee, J.; Zhang, Z. M.; King, W. P. Nanotopographical Imaging Using a Heated Atomic Force Microscope Cantilever Probe. *Sens. Actuators A* **2007**, *136*, 95–103.
25. Häeberle, W.; Pantea, M.; Hoerber, J. K. H. Nanometer-Scale Heat-Conductivity Measurements on Biological Samples. *Ultramicroscopy* **2006**, *106*, 678–686.
26. Kim, K. J.; King, W. P. Thermal Conduction between a Heated Microcantilever and a Surrounding Air Environment. *Appl. Therm. Eng.* **2009**, *29*, 1631–1641.
27. Park, K.; Cross, G. L. W.; Zhang, Z. M. M.; King, W. P. Experimental Investigation on the Heat Transfer between a Heated Microcantilever and a Substrate. *J. Heat Transfer* **2008**, *130*, 102401.
28. Schroeder, M. J.; Roland, C. M. Segmental Relaxation in End-Linked Poly(dimethylsiloxane) Networks. *Macromolecules* **2002**, *35*, 2676–2681.
29. Kong, Y.; Hay, J. N. Multiple Melting Behaviour of Poly(ethylene terephthalate). *Polymer* **2003**, *44*, 623–633.
30. Righetti, M. C.; Di Lorenzo, M. L.; Tombari, E.; Angiuli, M. The Low-Temperature Endotherm in Poly(ethylene terephthalate): Partial Melting and Rigid Amorphous Fraction Mobilization. *J. Phys. Chem. B* **2008**, *112*, 4233–4241.
31. Turner, P. S. Thermal-Expansion Stresses in Reinforced Plastics. *J. Res. Natl. Inst. Stand. Technol.* **1946**, *37*, 239–250.
32. Holliday, L.; Robinson, J. Thermal-Expansion of Composites Based on Polymers. *J. Mater. Sci.* **1973**, *8*, 301–311.
33. Feltham, S. J.; Yates, B.; Martin, R. J. The Thermal-Expansion of Particulate-Reinforced Composites. *J. Mater. Sci.* **1982**, *17*, 2309–2323.
34. Shevchenko, E. G.; Malyutina, T. I.; Borina, V. K.; Kafel, L. M. Thermal-Expansion of New Materials for Standard Measures. *Meas. Tech.* **1986**, *29*, 866–868.
35. Liu, X. J.; Yang, Y. W.; Yang, J. P. Direct Simulation Monte Carlo on Thermal Distribution of Rarefied Gas under Heated Atomic Force Microscope Nanoprobe. *J. Appl. Phys.* **2009**, *105*, 013508.
36. Rohsenow, W. M.; Hartnett, J. P.; Ganić, E. N. *Handbook of Heat Transfer Fundamentals*, 2nd ed.; McGraw-Hill Book Company: New York, 1985.
37. Van der Vegt, A. K.; Goveart, L. E. *Polymeren: van Keten tot Kunstof*, 5th ed.; VSSD: Delft, The Netherlands, 2005.
38. Bykov, V.; Gologanov, A.; Shevyakov, V. Test Sructure for SPM Tip Shape Deconvolution. *Appl. Phys. A* **1998**, *66*, 499–502.
39. Hua, Y.; Saxena, S.; Lee, J. C.; King, W. P.; Henderson, C. L. Direct Three Dimensional Nanoscale Thermal Lithography at High Speeds Using Heated Atomic Force Microscope Cantilevers. *Proc. SPIE* **2007**, *6517*, 65171L-1.
40. Kuo, C.; Chen, C. C.; Bannister, W. Microthermal Analysis of Rubber-Polyaniline Core−Shell Microparticles Using Frequency-Dependent Thermal Responses. *Thermochim. Acta* **2003**, *403*, 115–127.
41. Nelson, B. A.; King, W. P. Temperature Calibration of Heated Silicon Atomic Force Microscope Cantilevers. *Sens. Actuators A* **2007**, *140*, 51–59.